Hysteretic Behavior of RC Beams

By Alberto Carpinteri[1] and Andrea Carpinteri[2]

Abstract: A mechanical model for the cross section of a reinforced concrete beam is proposed. Attention is focused on the local phenomena relating to the cross section, while the phenomena relating to the beam element to which the section belongs is ignored. In particular the concrete fracturing mechanism and the slippage and yielding of steel are considered, while the smeared damage of concrete are not taken explicitly into account. Namely, a rigid-plastic constitutive law is assumed for steel, while for concrete a linear elastic one. Loading and unloading processes are considered, the bending moment range being lower than that of crack extension. The phenomenon of shake-down due to slippage or plastic deformation of the steel bars is studied. Up to a certain value of the bending moment an elastic shake-down occurs; above this value the shake-down becomes elastic-plastic and an hysteretic loop is described by the stress-strain diagram of steel. Thus the energy absorbed in such a dissipative phenomenon is computed for each loading cycle and some experimental results are reviewed.

Introduction

When a reinforced concrete beam is subjected to seismic, and generally repeated loadings, it deteriorates in a progressive manner and its stiffness and loading capacity sensibly decrease (3). Such effects are the result of different damage phenomena, like crushing and fracturing of concrete or pulling-out and yielding of the steel bars.

Several models have already been proposed with the aim of simulating the nonlinear behavior of reinforced concrete beams. For instance, the *dual component model,* where each member is replaced by an elastic element and an elasto-plastic element in parallel, the *fiber model,* where each section is divided into many layers of fibers and the moment-curvature relationship is determined by steel and concrete constitutive laws, the *single component model,* where each member is represented by an elastic beam element with inelastic springs (hinges) at its two ends (1). These models do not distinguish the contribution of each damage mechanism, but they are intended to represent a global effect.

In the present paper, a mechanical model for the cross section of a reinforced concrete beam will be proposed. The attention will be focused on the local phenomena relating to the cross section, while the phenomena relating to the beam element to which the section belongs will be ignored. In particular, the concrete fracturing mechanism and the slippage and yielding of steel will be considered, while the smeared damage of concrete will not be taken explicitly into account. Namely, a rigid-plastic constitutive law will be assumed for steel, while for concrete, a

[1]Research Asst., Istituto di Scienza delle Costruzioni, University of Bologna, 2 Viale Risorgimento, 40136 Bologna, Italy.

[2]Post-doctoral Fellow, Istituto di Science delle Costruzioni, University of Bologna, 2 Viale Risorgimento, 40136 Bologna, Italy.

Note.—Discussion open until February 1, 1985. To extend the closing date one month, a written request must be filed with the ASCE Manager of Technical and Professional Publications. The manuscript for this paper was submitted for review and possible publication on August 19, 1982. This paper is part of the *Journal of Structural Engineering,* Vol. 110, No. 9, September, 1984. ©ASCE, ISSN 0733-9445/84/0009-2073/$01.00. Paper No. 19148.

linear elastic one, coupled with a crack propagation condition according to Fracture Mechanics Theory (13). A more realistic concrete model should in fact simulate an elasto-softening behavior (8), with the possibility of a crushing collapse. However, the proposed model is able to predict, with sufficient accuracy, the order of magnitude of some interesting quantities, such as the dissipated energy in one loading cycle.

More precisely, a reinforced concrete beam section with a through-thickness edge crack in the stretched part will be considered. The force transmitted by the reinforcement to the beam can be estimated by means of a rotation congruence condition (5). Applying Linear Elastic Fracture Mechanics, such a force increases linearly by increasing the applied bending moment, until the limit force of pulling-out or yielding of steel is reached. From this point onwards, a perfectly plastic behavior of the reinforcement can be considered. In fact, it is possible to show that even the slippage is describable by a rigid-plastic law (7) and the bond stress-slip relationship for monotonic loading in tension is almost identical to that in compression (6).

Once the bending moment of slippage or yielding has been exceeded, the cracked beam section presents a linear-hardening behavior, until the concrete fracture also occurs (5).

Loading and unloading processes will be considered, the bending moment range being lower than that of crack extension. The phenomenon of shake-down due to slippage or plastic deformation of the steel bars will be studied. Up to a certain value of the bending moment an elastic shakedown occurs; above this value the shake-down becomes elastic-plastic and an hysteretic loop is described by the stress-strain diagram of steel. Thus the energy absorbed in such a dissipative phenomenon will be computed for each loading cycle.

Behavior of Beam-Section Under Monotonic Loadings

Let us consider a reinforced concrete beam element of length $\Delta l \rightarrow 0$, with a rectangular cross section of thickness t and depth b, subjected to a bending moment M (Fig. 1). Let the steel reinforcement be distant h from the external surface, and a through-thickness edge crack of depth $a \geq h$ is assumed to exist in the stretched part (Fig. 1). Therefore the cracked concrete beam element will be in all subjected to the bending moment M and to the eccentric axial force F, due to the statically un-

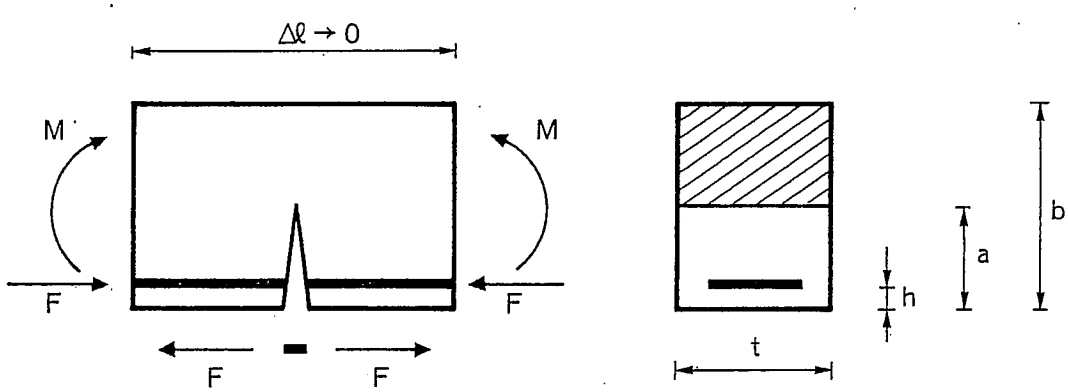

FIG. 1.—Cracked Reinforced Beam Element

determined reaction of the reinforcement.

It is well-known that, while an uncracked section performs an internal action of perfectly fixed joint [Fig. 2(*a*)], a cracked section is equivalent to an elastic joint, rotating under the action of the bending moment $M*$ and the axial force F^* [Fig. 2(*b*)] (5):

$$\phi = \lambda_{MM} M^* + \lambda_{MF} F^* \quad (1)$$

in which $\lambda_{MM} = 2/b^2 tE \int_0^\xi Y_M^2(\xi)\,d\xi$; and $\lambda_{MF} = 2/btE \int_0^\xi Y_M(\xi) Y_F(\xi)\,d\xi$. Applying a rotation congruence condition (5), the statically undetermined force F, transmitted by the reinforcement [Figs. 1, 2(*b*)] can be computed as a function of the applied moment M:

$$\frac{Fb}{M} = \frac{1}{\left(\frac{1}{2} - \frac{h}{b}\right) + r(\xi)}, \quad (2)$$

$$\text{in which:} \quad r(\xi) = \frac{\int_0^\xi Y_M(\xi)\, Y_F(\xi)\, d\xi}{\int_0^\xi Y_M^2(\xi)\, d\xi}, \quad \text{with:} \quad \xi = \frac{a}{b},$$

$$Y_M(\xi) = 6 \times (1.99\,\xi^{1/2} - 2.47\,\xi^{3/2} + 12.97\,\xi^{5/2} - 23.17\,\xi^{7/2} + 24.80\,\xi^{9/2}),$$

$$\text{for} \quad \xi \le 0.7, \; Y_F(\xi) = 1.99\,\xi^{1/2} - 0.41\,\xi^{3/2} + 18.70\,\xi^{5/2} - 38.48\,\xi^{7/2}$$

$$+ 53.85\,\xi^{9/2}, \quad \text{for} \quad \xi \le 0.7 \quad (3)$$

From Eq. 2, it is possible to obtain the bending moment of plastic flow for the reinforcement:

$$M_P = F_p b \left[\left(\frac{1}{2} - \frac{h}{b}\right) + r(\xi)\right] \quad (4)$$

F_p can indicate either the force of yielding $f_y A_S$ or the force of pulling-out, when the latter is lower than the former, as on the other hand very often happens.

For $M \le M_P$ the relative rotation of the cracked section is zero, while for $M > M_P$ Eq. 1 gives:

$$\phi(M) = \lambda_{MM}\left[M - F_P\left(\frac{b}{2} - h\right)\right] - \lambda_{MF} F_P \quad (5)$$

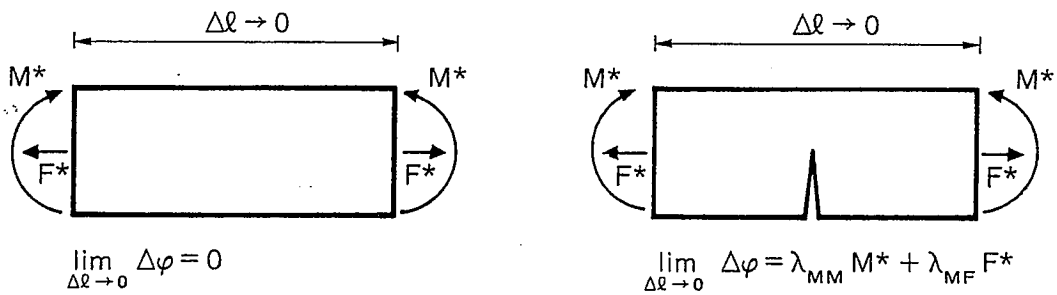

FIG. 2.—Local Rotation in Cracked and Uncracked Beam Cross Section

This relationship represents the equivalence of the cracked section with a rigid-linear hardening hinge (5). By increasing the crack depth ξ, the hardening line becomes more and more inclined, until giving rigid-perfectly plastic behavior.

Elastic-Plastic Shake-Down Under Repeated Loadings

Since the analysis of the preceding section exclusively concerns a cracked section, or at most, a cracked beam element of infinitesimal length, it is coherent to hypothesize a rigid-perfectly plastic behavior of the reinforcement.

If the cracked section is assumed to be cyclically loaded and unloaded and the crack extension possibility is ignored for the moment, we have the three following fields of steel behavior (Fig. 3): (1) $0 \leq M \leq M_P$: elastic behavior; (2) $M_P < M \leq M_{SD}$: elastic shake-down; and (3) $M_{SD} < M$: plastic shake-down. The unknown element of the problem is the moment M_{SD}, above which the shake-down becomes plastic and the steel stress-strain curve presents hysteretic cycles and energy dissipation (Fig. 3).

If the cracked section is loaded with a moment M, a little higher than M_P, and then it is unloaded, a residual rotation remains, which, in the limit-case of rigid-perfectly plastic reinforcement, coincides with the under loading rotation $\phi(M)$. In this case constraint between steel and concrete occurs, i.e. the concrete element compresses the steel segment, which works as a strut [Fig. 4(*b*)]. Therefore we can assume that the unknown compression F produces the rotation $\phi(F)$ in the cracked section.

Thus, when the reinforcement is rigid-perfectly plastic, the following condition holds:

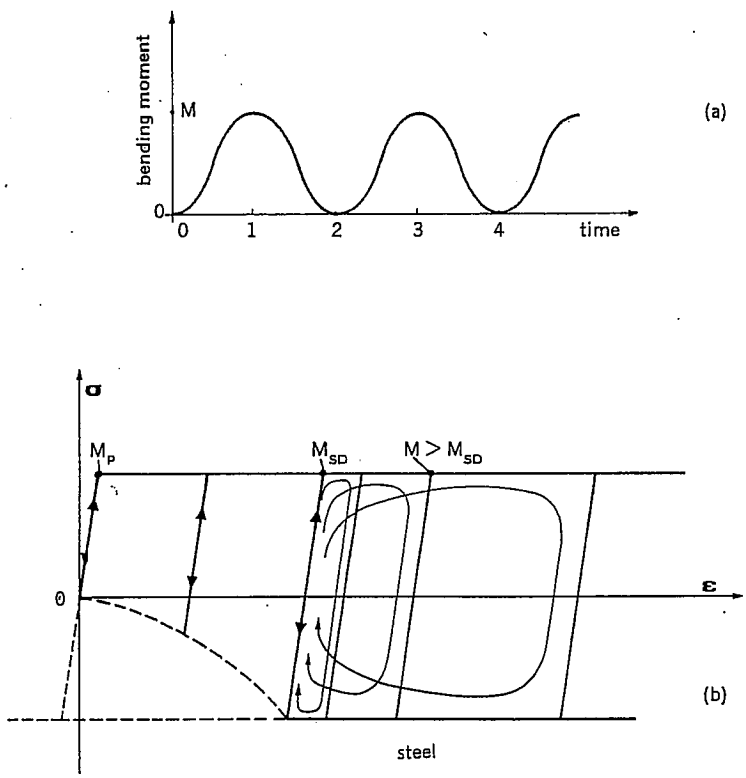

FIG. 3.—Hysteretic Loops in Steel Stress-Strain Curve

$$\phi(M) = \phi(F), \quad (6)$$

from which the unknown F can be extracted, that is the steel compression, when the beam-section has been unloaded. The moment of plastic shake-down M_{SD} is defined as the lowest moment for which $F = F_P$, i.e., for which the steel yields even in compression after unloading.

Now Eq. 6 will be made explicit. Rotation $\phi(M)$ due to the bending moment M, $M > M_P$ [Fig. 4(*a*)], is given by Eq. 5, while rotation $\phi(F)$ produced by the force F after unloading is [Fig. 4(*b*)]:

$$\phi(F) = \lambda_{MM} F\left(\frac{b}{2} - h\right) + \lambda_{MF} F \quad (7)$$

Applying Eq. 6 one obtains:

$$F = M \frac{\lambda_{MM}}{\lambda_{MM}\left(\frac{b}{2} - h\right) + \lambda_{MF}} - F_P \quad (8)$$

If both the members of Eq. 8 are divided by F_P and Eq. 4 is recalled, the following linear relationship, connecting the external bending moment M with the compression F after unloading, results:

$$\frac{F}{F_P} = \frac{M}{M_P} - 1 \quad (9)$$

A graphic representation of such a connection is reported in Fig. 5. For $M \leq M_P$, of course, the steel compression after unloading is equal to zero, while for $M = M_{SD} = 2M_P$ the reverse steel yielding after unloading begins to happen. Observe that ratio 2, between the moment of

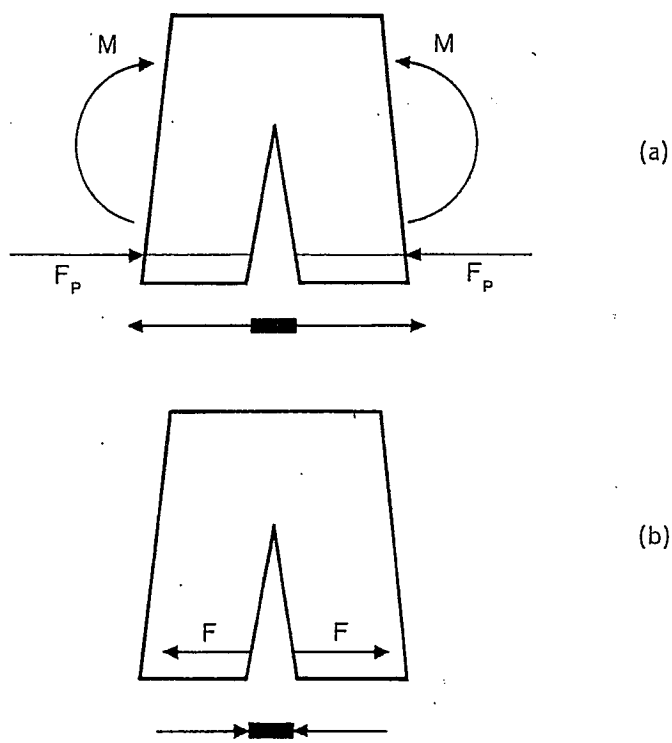

FIG. 4.—Statical Schemes: (*a*) Under Loading; and (*b*) After Unloading for Reinforced Beam Cross Section

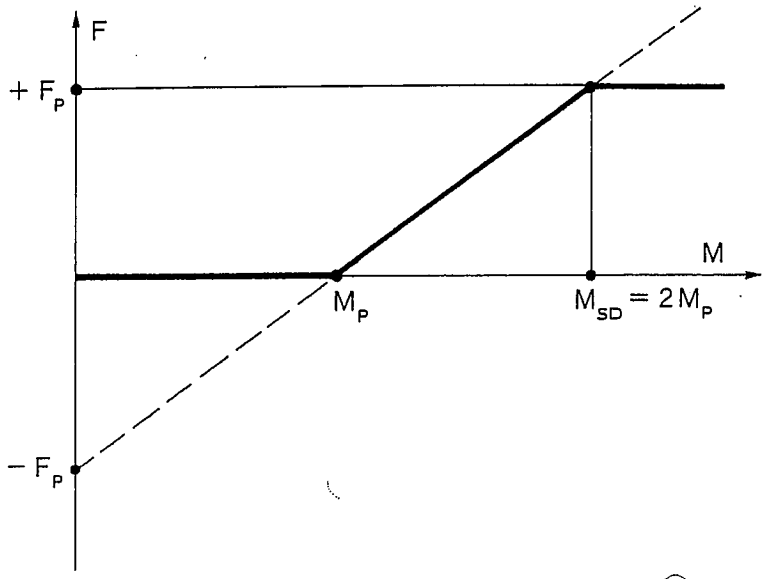

FIG. 5.—Compression Force after Unloading Against Maximum Applied Bending Moment

plastic shake-down M_{SD} and the moment of direct plastic flow M_P, is the same as that which results in the case of the well-known simple model with in-parallel elements of Fig. 6.

The arguments developed up to now are valid only if the crack extension does not precede the plastic shake-down:

$$M_{SD} = 2M_P < M_F \quad (10)$$

M_F being the moment of crack extension (5). In the opposite case, the elastic shake-down will occur for $M_P < M < M_F$, while the plastic shake-down is impossible. Recalling Fig. 9 of Ref. 5, it is possible to specify that the plastic fatigue can theoretically occur only for sufficiently low values of the number $N_P = (f_y b^{1/2}/K_{IC})A_s/A$, where K_{IC} is the concrete fracture toughness. In the case of high N_P numbers, the model than predicts the possibility of a nonlinear combined effect of stable progressive fracture in concrete and shake-down in steel (5).

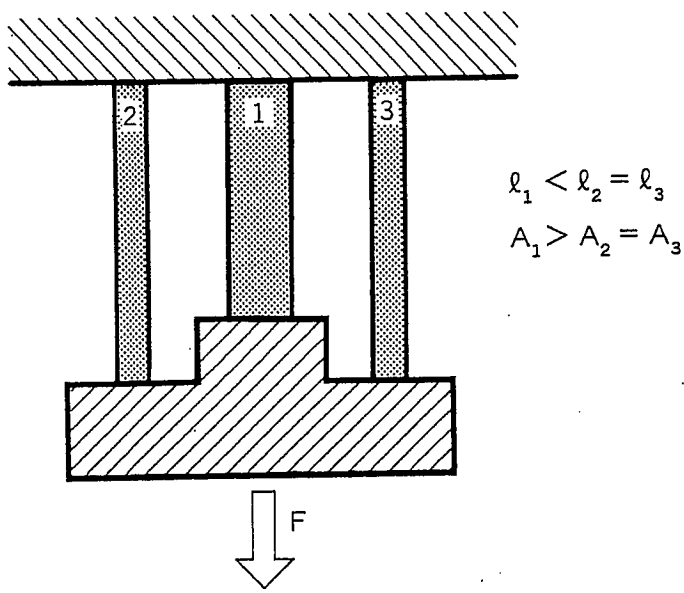

FIG. 6.—Simplified Shake-Down Model with In-Parallel Elements

Consider now the case $M > M_{SD}$ (Fig. 7). Once the beam-section has been unloaded, the residual rotation is reduced to that related to the moment M_{SD}. More precisely, unloading with constant rotation occurs at first (line 1-2 of Fig. 7) and then the plastic flow of the compressed steel up to the equilibrium situation (line 2-3). When the moment is increased again, the moment M_{SD} is reached, at first the rotation being constant (line 3-4), and then the final moment M, the rotation increasing linearly in this second stage (line 4-1).

As Fig. 7 makes evident, the point representative of the system on the plane M-ϕ describes—during a loading cycle—a closed curve, which, when $M < M_{SD}$, degenerates into a segment. It is therefore quite easy to compute the plastic energy dissipated in each cycle; it is equal to the area of the rectangular trapezium of Fig. 7:

$$\frac{\text{work}}{\text{cycle}} = \frac{1}{2}(M + 2M_P)[\phi(M) - \phi(2M_P)] \quad \text{(11)}$$

Recalling Eqs. 4 and 5 we get:

$$\frac{\text{work}}{\text{cycle}} = \frac{1}{2}\frac{2}{b^2 tE}\int_0^{\xi} Y_M^2(\xi)\,d\xi \cdot \left[M^2 - 4F_P^2 b^2\left(\frac{1}{2} - \frac{h}{b} + r(\xi)\right)^2\right] \quad \text{(12)}$$

which in nondimensional form appears as

$$\frac{\text{work/cycle}}{b^2 tE} = \int_0^{\xi} Y_M^2(\xi)\,d\xi \cdot \left[\left(\frac{M}{b^2 tE}\right)^2 - 4\left(\frac{F_P b}{b^2 tE}\right)^2\left(\frac{1}{2} - \frac{h}{b} + r(\xi)\right)^2\right] \quad \text{(13)}$$

and in a more compact form:

$$\frac{\text{work/cycle}}{b^2 tE} = \int_0^{\xi} Y_M^2(\xi)\,d\xi \cdot \left[\left(\frac{M}{b^2 tE}\right)^2 - \left(\frac{M_{SD}}{b^2 tE}\right)^2\right] \quad \text{(14)}$$

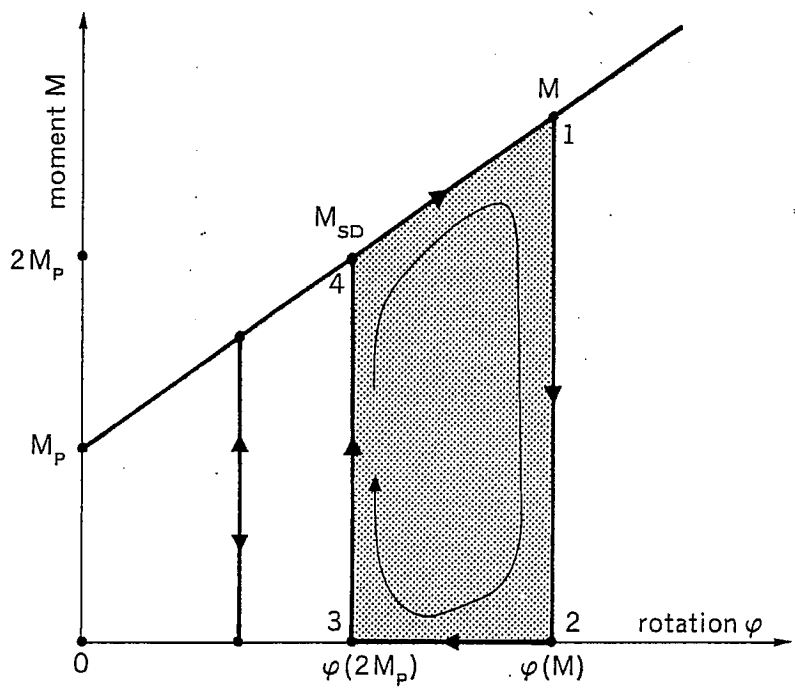

FIG. 7.—Hysteretic Loop in Moment-Rotation Diagram, under Unidirectional Cyclic Loading

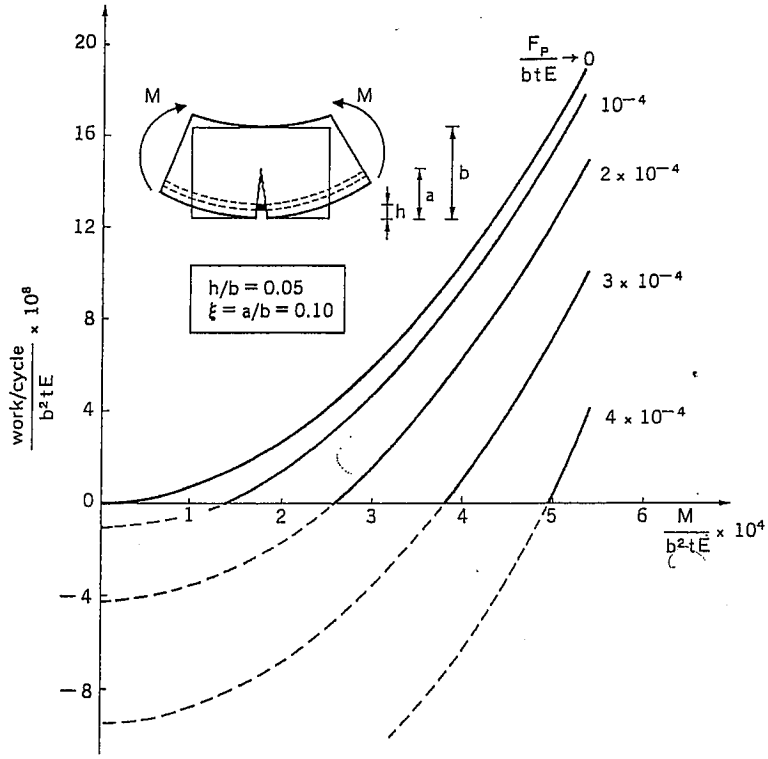

FIG. 8.—Dissipated Energy per Cycle Against Maximum Bending Moment, Varying Parameter F_P/btE

In Fig. 8 the dissipated energy per cycle is reported as a function of the maximum bending moment and varying the parameter F_P/btE. Obviously, it increases quadratically by increasing the moment and decreases by increasing F_P/btE. The points, where the curves intersect the abscissae axis, represent the moment M_{SD}, as Eq. 14 explicitly shows.

In Fig. 9 the dissipated energy per cycle is reported as a function of the crack depth ξ and varying the parameter F_P/btE. It increases with ξ in a monotonic way.

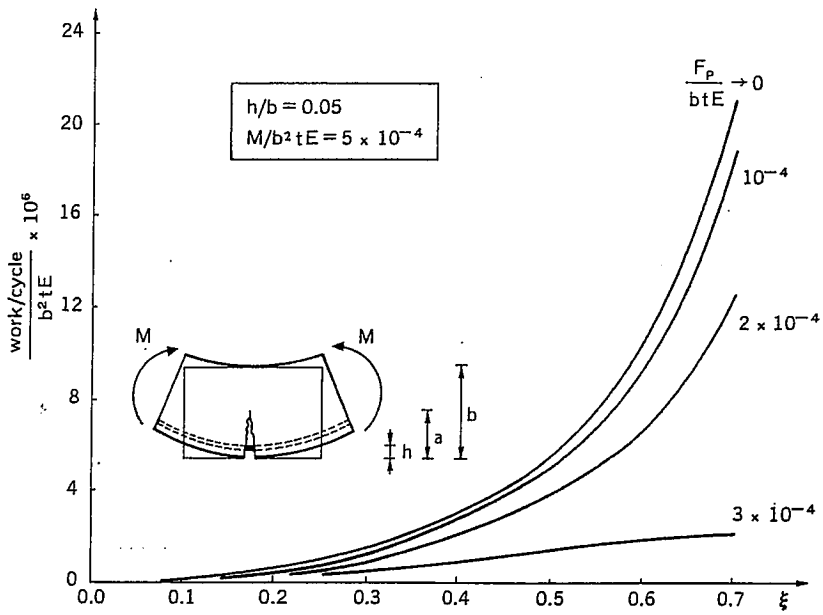

FIG. 9.—Dissipated Energy per Cycle against Crack Depth ξ, Varying Parameter F_P/btE

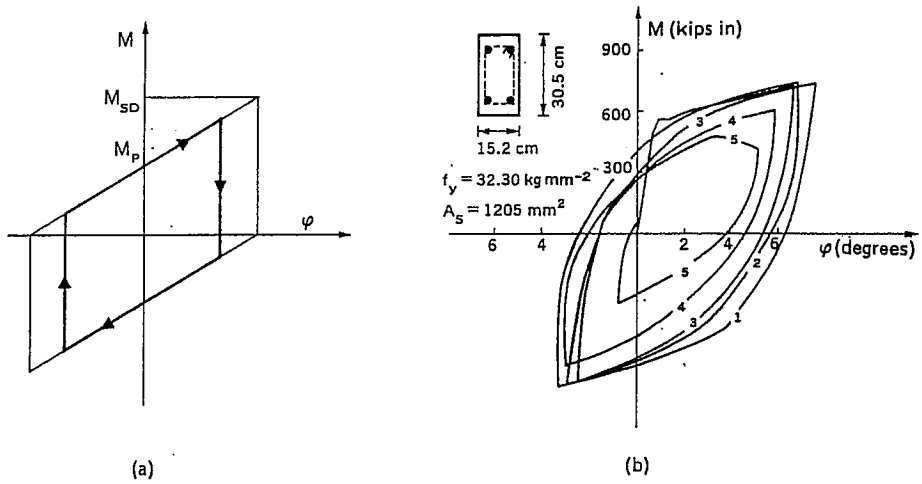

FIG. 10.—Hysteretic Behavior of Moment-Rotation Diagram, under Reversed Cyclic Loading: (*a*) Theoretical Prediction when $M_P \leq M \leq M_{SD}$; and (*b*) Experimental Confirmation (3)

In the case of doubly reinforced beam-section subjected to cyclic loadings, the considered model predicts an hysteretic behavior as that of Fig. 10(*a*), when $M_P \leq M \leq M_{SD}$, as well as that of Fig. 11(*a*), when $M > M_{SD}$ (see Fig. 7). It should be observed that the theoretical behavior of Fig. 10(*a*) is qualitatively similar to the experimental one of Fig. 10(*b*) (3). In the latter, however, further degradation phenomena are present, which the proposed model is not able to predict. On the other hand Eq. 4 gives the following value of steel yielding moment, in relation to the case of Fig. 10(*b*) (3) and for $\xi = h/b \simeq 0.1$ (this means that a crack deep up to the reinforcement is assumed):

$$M_P = 0.6F_P b = 0.6 f_y A_S b = 0.6 \times 32.30 \text{ kg mm}^{-2} \times 1{,}205 \text{ mm}^2$$

$$\times 305 \text{ mm} = 7{,}122{,}634 \text{ kg mm} = 618 \text{ kips in.}$$

Such a value is very close to the experimental result [Fig. 10(*b*)].

The dissipated energy in one loading cycle, when the maximum and the minimum bending moments are respectively $+M_{SD}$ and $-M_{SD}$, can be evaluated by considering the M-ϕ diagram of Fig. 12:

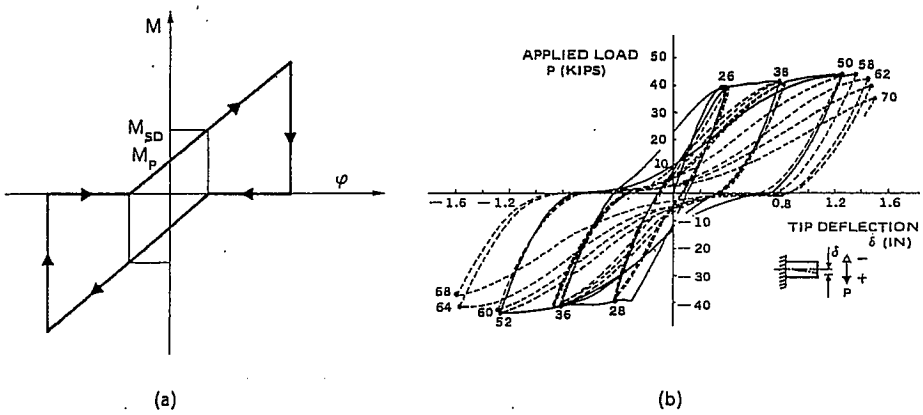

FIG. 11.—Hysteretic Behavior of Moment-Rotation Diagram, under Reversed Cyclic Loading: (*a*) Theoretical Prediction when $M > M_{SD}$; and (*b*) Experimental Confirmation (11)

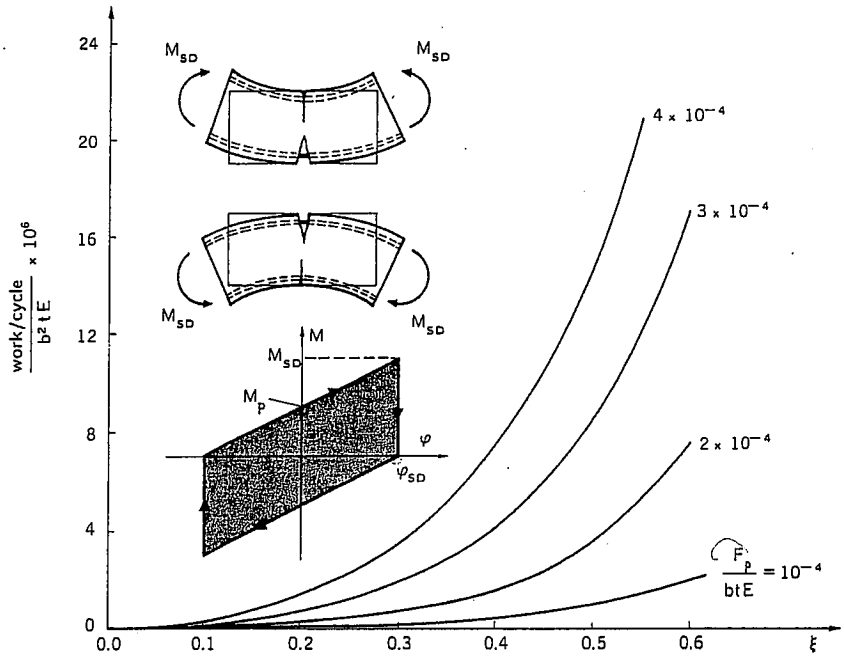

FIG. 12.—Dissipated Energy per Cycle under Reversed Loading Against Crack Depth ξ, Varying Parameter F_P/btE

$$\frac{\text{work}}{\text{cycle}} = 2M_{SD}\phi_{SD} \quad \ldots\ldots\ldots\ldots\ldots\ldots\ldots\ldots\ldots\ldots \quad (15)$$

Recalling that

$$\phi_{SD} = \lambda_{MM}M_P, \quad \text{and,} \quad M_{SD} = 2M_P, \quad \text{we get:} \quad \frac{\text{work}}{\text{cycle}} = 4\,M_P^2\lambda_{MM} \ldots \quad (16)$$

which in nondimensional form becomes:

$$\frac{\text{work/cycle}}{b^2tE} = 8\left(\frac{F_P}{btE}\right)^2\left(\frac{1}{2} - \frac{h}{b} + r(\xi)\right)^2 \int_0^{\xi} Y_M^2(\xi)\,d\xi \ldots\ldots\ldots\ldots\ldots \quad (17)$$

In Fig. 12, the dissipated energy per cycle is displayed by varying the crack depth ξ and the parameter F_P/btE. It is interesting to verify that the order of magnitude of the energy dissipated in the experimental case of Fig. 10(*b*) is the same as that predicted by the theoretical model. It is also possible to determine the crack depth ξ_0 for which we have the coincidence of the two values. For the experimental case of Fig. 10(*b*), we have the parameter: F_P/btE = (85,919 lb)/(12 in.) × (6 in.) × (4,272 ksi) = (0.381 MN)/(0.305 m) × (0.152 m) × (29,434 MPa) $\simeq 2.8 \times 10^{-4}$, and the dimensionless energy: work/cycle/b^2tE = (1,400 kips in.) × (6°/360°) × 6.28/(12 in.)^2 × (6 in.) × (4,272 ksi) = (0.158 MNm) × (6°/360°) × 6.28/(0.305 m)^2 × (0.152 m) × (29,434 MPa) $\simeq 39.7 \times 10^{-6}$.

Therefore, we can assert that the experimental dissipated energy coincides with the theoretical one when the crack depth is $\xi_0 \simeq 0.7$ (Fig. 12). This means that the theoretical model is able to predict the experimental dissipated energy exactly only when the cross section is completely disconnected ($\xi_0 > 0.5$). In fact, the interlocking of the two free surfaces and the steel dowel action will contribute to hold the two beam segments together and to present a compressed part at every loading

cycle. Then, more generally, we can say that the obtained crack depth ξ_0 can represent a measure of the damage level in the concrete cross-section.

The theoretical behavior of Fig. 11(*a*) is then analogous to the experimental one of Fig. 11(*b*) (11), which shows considerable concavities of the cycle in the second and fourth quadrant.

Concluding Remarks

1. The considered Fracture Mechanics model does not claim to describe every aspect of reality; it only means to explain those, which cannot be explained by means of the traditional concepts of Solid Mechanics (stress, strain, displacements, . . .).

2. Cracks grow in reinforced concrete beams before steel yielding, only when slippage is allowed between concrete and steel. Even if slippage is not explicitly considered in the model, it can be simulated by a fictitious yield strength $\bar{f}_y$ of steel, lower than the real f_y [e.g. $\bar{f}_y \sim 0.1\, f_y$ in (7)].

3. It is coherent to consider the reinforcement as rigid-perfectly plastic rather than elastic-perfectly plastic, since the proposed model represents only the behavior of a cracked section, or—at the most—of a cracked beam element of infinitesimal length. On the other hand, several efforts were made in order to derive the plastic rotation by integration of curvatures, but the tests showed that it is caused by a concentrated rupture mechanism (4).

4. The fracturing process has been analyzed up to the relative crack depth 0.6. On the other hand the presented diagrams make clear the trends of the model even for higher depths.

5. A linear elastic constitutive law has been assumed for concrete, coupled with a fracture condition. Namely the process zone size is a small percentage of crack length at crack tip instability. In tests on concrete (12), the process zone size has been observed to be only a few millimeters in length. Thus, when the computed stress-intensity factor K_I reaches the value of the concrete fracture toughness K_{IC}, a necessary and sufficient condition for local instability is met. Moreover, as has numerically been demonstrated by Saouma and Ingraffea (12), most of the overall structural nonlinearity stems from concrete cracking, and only towards failure does concrete softening play a substantial role.

Appendix I.—References

1. Banon H., Biggs, J. M., Irvine, H. M., "Seismic Damage in Reinforced Concrete Frames," *Journal of the Structural Division*, ASCE, Vol. 107, No. ST9, 1981, pp. 1713–1729.
2. Blaauwendraad, J., Grootenboer, H. J., "Essentials for Discrete Crack Analysis," Advanced Mechanics of Reinforced Concrete, IABSE-Colloquium Final Report, Delft, The Netherlands, 1981, pp. 263–272.
3. Brown, R. H., and Jirsa, J. O., "Reinforced Concrete Beams Under Load Reversal," *American Concrete Institute Journal*, May, 1971, pp. 380–390.
4. Cantù, E., and Macchi, G., "Plastic Rotations by Local Analysis," Advanced Mechanics of Reinforced Concrete, IABSE-Colloquium Final Report, Delft, The Netherlands, 1981, pp. 521–530.
5. Carpinteri, A., "Stability of Fracturing Process in R.C. Beams," *Journal of*

Structural Engineering, ASCE, Vol. 110, No. 3, 1984, pp. 544–558.
6. Ciampi, V., Eligehausen, R., Bertero, V., and Popov, E., "Analytical Model for Deformed Bar Bond under Generalized Excitations," Advanced Mechanics of Reinforced Concrete, IABSE-Colloquium Final Report, Delft, The Netherlands, 1981, pp. 53–67.
7. Giuriani, E., "Experimental Investigation on the Bond-Slip Law of Deformed Bars in Concrete," Advanced Mechanics of Reinforced Concrete, IABSE-Colloquium Final Report, Delft, The Netherlands, 1981, pp. 121–142.
8. Hillerborg, A., Modéer, M., and Petersson, P. E., "Analysis of Crack Formation and Crack Growth in Concrete by Means of Fracture Mechanics and Finite Elements," *Cement and Concrete Research*, Vol. 6, 1976, pp. 773–782.
9. Noguchi, H., "Non-linear Finite Elements Analysis of Reinforced Concrete Beam-Column Joints," Advanced Mechanics of Reinforced Concrete, IABSE-Colloquium Final Report, Delft, The Netherlands, 1981, pp. 639–654.
10. Plauk, G., and Hees, G., "Finite Element Analysis of Reinforced Concrete Beams with Special Regard to Bond Behaviour," Advanced Mechanics of Reinforced Concrete, IABSE-Colloquium Final Report, Delft, The Netherlands, 1981, pp. 655–670.
11. Popov, E. P., "Seismic Behavior of Structural Subassemblages," *Journal of the Structural Division*, ASCE, Vol. 106, No. ST7, 1980, pp. 1451–1474.
12. Saouma, V. E., and Ingraffea, A. R., "Fracture Mechanics Analysis of Discrete Cracking," Advanced Mechanics of Reinforced Concrete, IABSE-Colloquium Final Report, Delft, The Netherlands, 1981, pp. 413–436.

Appendix II.—Notation

The following symbols are used in this paper:

A = total area of cross section;
A_S = steel area;
a = crack depth;
b = depth of beam;
E = Young's modulus of concrete;
F = statically undetermined reaction of reinforcement;
$F_P = f_y A_s$ = force of plastic flow for reinforcement;
f_c = compressive strength of concrete;
f_u = tensile strength of concrete;
f_y = yield strength of steel;
h = distance of reinforcement from external surface;
K_I = stress-intensity factor;
K_{IC} = fracture toughness of concrete;
M = bending moment;
M_F = bending moment of crack propagation;
M_P = bending moment of steel plastic flow;
M_{SD} = bending moment of plastic shake-down;
N_P = $f_y b^{1/2}/K_{IC} \cdot A_s/A$ = nondimensional number;
r = ratio defined in Eq. 3;
t = thickness of beam;
Y_M, Y_F = functions defined in Eq. 3;
$\xi = a/b$ = relative crack depth;
$\lambda_{MM}, \lambda_{MF}$ = rotational compliances due to bending moment and axial force; and
ϕ = local rotation.